ACS APPLIED NANO MATERIALS
Cite This: ACS Appl. Nano Mater. 2019, 2, 2542−2547
Article
www.acsanm.org

New Promesogenic Ligands for Host Medium Microencapsulation by Quantum Dots via Liquid Crystal Phase Transition Templating

Amir Keshavarz,[†] Sheida T. Riahinasab,[‡] Linda S. Hirst,*[,‡] and Benjamin J. Stokes*[,†]

[†]Department of Chemistry & Chemical Biology and [‡]Department of Physics, University of California, Merced, 5200 N. Lake Road, Merced, California 95343, United States

Supporting Information

ABSTRACT: The design, synthesis, properties, and performance of a new class of promesogenic calamitic side-tethering organic ligands used to direct quantum dot nanoparticle self-assembly are described. This work was motivated by inadequate modularity, step count, and yield associated with syntheses of existing ligands. Attaching the new ligands to quantum dots and dispersing them in a liquid crystal host affords hollow micrometer-sized capsules via phase transition templating. The capsules resist thermal decomposition up to 350 °C—significantly higher than any previously reported microcapsules assembled from side-tethering calamitic ligand-functionalized nanoparticles. These novel ligands can be used for encapsulation applications where stability under high temperature is required. Evaluation of the capsules by small-angle X-ray scattering shows that interparticle spacing varies from 10 to 13 nm depending on the ligand used and is correlated to aminoalkyl chain length.

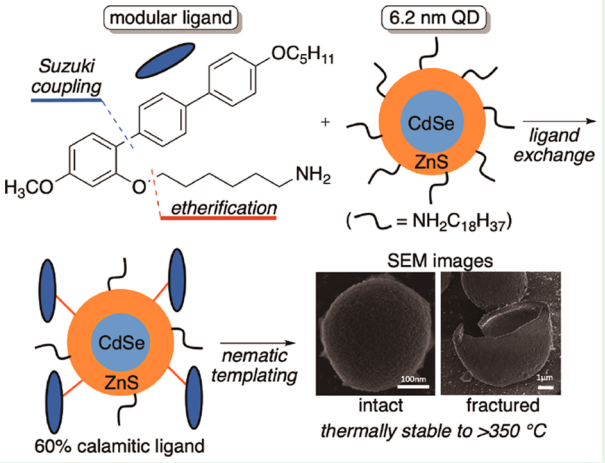

KEYWORDS: *encapsulation, nematic templating, self-assembly, promesogenic ligands, organic synthesis, quantum dots, thermostable capsules, ligand exchange*

INTRODUCTION

A wide variety of small organic molecules have been employed as surface-modifying ligands for metallic or semiconducting nanoparticles.[1−5] Metal nanoparticles functionalized with mesogenic (liquid crystalline) or promesogenic organic ligands bearing a motif consisting of multiple closely linked aromatic rings—likened to a molecular "rod" (calamitic)—and an orthogonal nucleophilic tethering arm self-assemble[6] into different two- and three-dimensional mesoscale morphologies like rods, spheres, and capsules (Figure 1).[3,7,12] The derived morphologies are envisioned for use in biochemical sensors,[13,14] optoelectronic and photovoltaic devices,[15−18] and light-emitting diodes.[19] Rather few side-attaching ligands have been systematically evaluated as mediators of nanoparticle self-assembly. In one example, using three different ligands, Pociecha and co-workers showed that varying the length of the alkyl chain connected to the thiol in **A** can direct the self-assembly of the resultant ligand-modified gold nanoparticles into various morphologies upon evaporation of toluene.[20] More commonly, only one ligand is evaluated. Examples include thiol **B**,[21] related ligands[22] and proligands,[23,24] and our own ligand **C**.[8] After attaching **C** to core−shell quantum dots, micrometer-sized discrete capsules form following nucleation and growth of the nematic phase at the isotropic−nematic transition temperature of a liquid crystal host, such as 4-cyano-4′-pentylbiphenyl (colloquially known as "5CB")[8,12]—a process we refer to as nematic templating. Recently this methodology was expanded to the formation of solid closed-cell foams and tubular networks.[25] The process takes

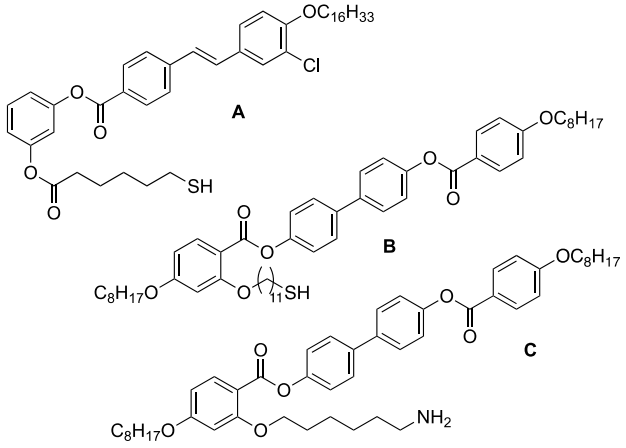

Figure 1. Calamitic ligands used for ligand-modified metal nanoparticle self-assembly.

Received: March 13, 2019
Accepted: March 19, 2019
Published: March 19, 2019

DOI: 10.1021/acsanm.9b00476
ACS Appl. Nano Mater. 2019, 2, 2542−2547

Table 1. Ligand Library Synthesis

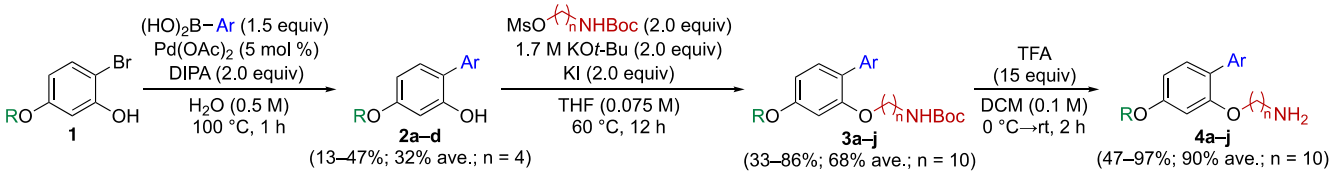

Combined three-step yields are reported. Isolated yields of the individual steps are listed in parentheses in the order of the reaction sequence above.

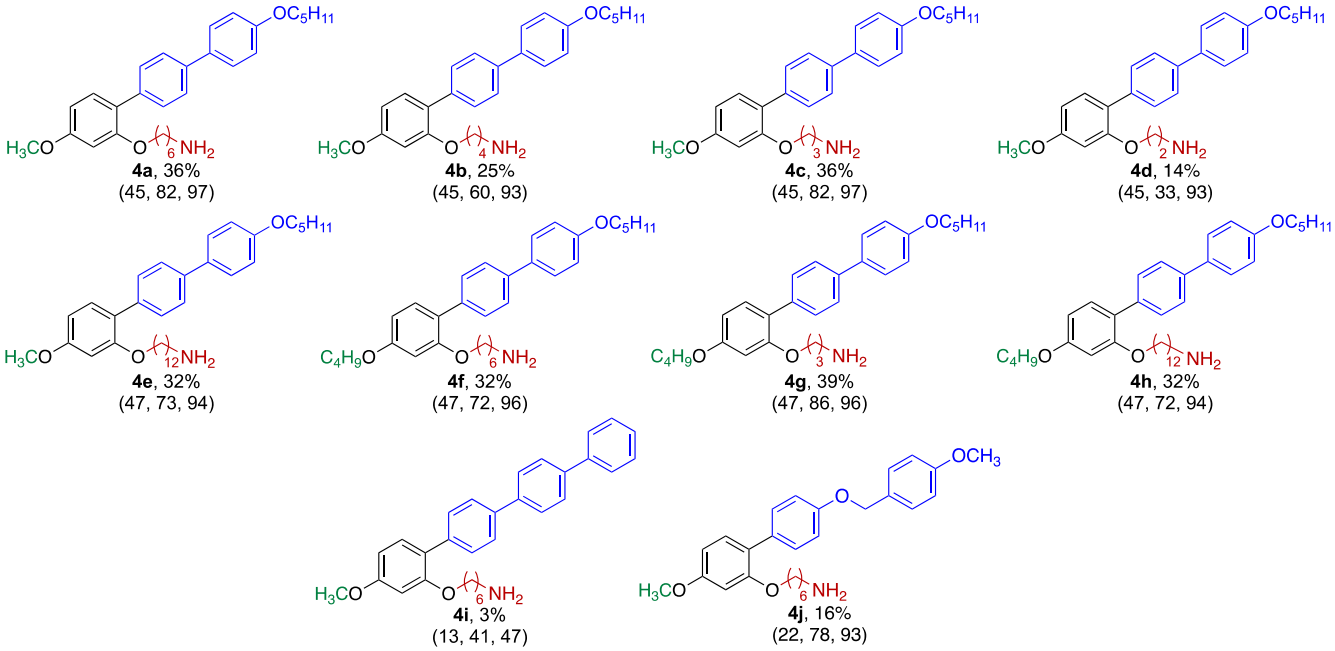

advantage of the differential solubility of the ligand-modified particles in the nematic and isotropic phases of a liquid crystal host medium (in particular, the aforementioned 5CB). Initially, ligand-modified nanoparticles are uniformly dispersed in the isotropic phase. The composite system is then cooled rapidly into the nematic phase, whence phase nucleation, followed by growth within the shrinking isotropic domains, results in particle segregation to the domain interfaces, and consequently a variety of hollow structures,[25] including the microcapsules reported here.

Hollow micrometer-scale capsules constructed from closely packed quantum dots[9] and metallic nanoparticles[11] have been previously demonstrated by our group using ligands designed for low-temperature encapsulation applications. Metallic nanoparticle capsules were designed to produce an optically triggered release by taking advantage of plasmonic heating. For the new ligand series reported herein, we employ a novel ligand core structure designed to form capsules by the same mechanism, while supporting high-temperature applications. The new capsules are much more robust to extreme temperatures, yet still amenable to controlled release by alternative methods, such as mechanical shear. Owing to a more calamitic ligand core, stronger $\pi-\pi$ interaction is possible between the nanoparticles.

Studies limited to single ligands are prohibited from uncovering any relationship between ligand structure and nanoparticle self-assembly behavior, but challenges with ligand synthesis and purification make this all too common. Anecdotally, we have experienced many challenges with the synthesis and purification of **C**, which is prepared in eights steps with a longest linear sequence of five steps.[8] Like **A** and **B**, ligand **C** also contains esters in the calamitic arm, which are prone to decompose upon attack by a nitrogen atom in particular. Fortunately, these esters are not critical for nanoparticle self-assembly (in fact, they may be detrimental); they are likely relics of the condensation reactions used for their synthesis. They also provide structural degrees of freedom that make the calamitic motif less rodlike than if the arenes were directly linked. Thus, given the broad utility of calamitic side-attaching ligands, and the wealth of information that could be obtained from structure−self-assembly relationships, we endeavored to prepare a modular, scalable, ester-free ligand library featuring direct arene−arene linkages, which we hypothesized would result in bulk crystallinity rather than liquid crystallinity, and thereby encourage stabilizing interparticle $\pi-\pi$ interactions when bound to nanoparticles, leading to stronger nanoparticle mesostructures. Herein, we describe the development of a library of calamitic side-tethering ligands by modifying the calamitic arm, amine tether length, and ethereal linker lengths, and we demonstrate their ability to direct quantum dot self-assembly into microcapsules stable up to 350 °C via nematic templating.

RESULTS AND DISCUSSION

Our synthetic design starts from commercially available bromophenols (**1**, Table 1), to which aromatic groups (blue) could be coupled, followed by attachment of the tethering arm (red). We designed a ten-membered library of ligands (**4a**−**4j**, Table 1) to evaluate their ability to attach to CdSe/ZnS core−shell quantum dots and direct their self-assembly. Ligand **4a**

DOI: 10.1021/acsanm.9b00476
ACS Appl. Nano Mater. 2019, 2, 2542−2547

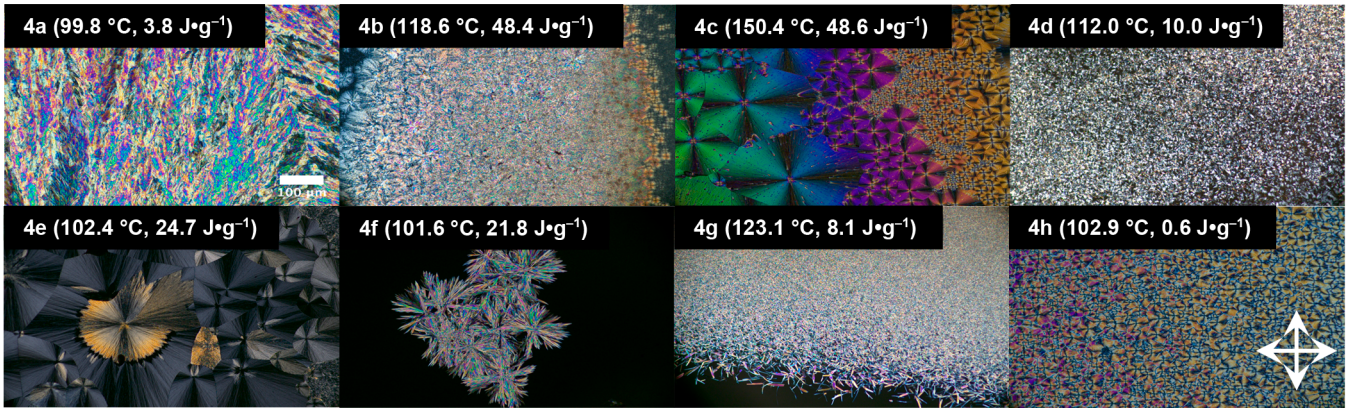

Figure 2. Birefringence textures of **4a**−**4h** observed using polarized optical microscopy (10× objective). The transition temperature (T_{trans}) and latent heat (ΔH_{trans}) of the only observed differential scanning calorimetry event for each ligand are included in parentheses. Crossed arrows indicate polarizer directions.

was envisioned as our parent ligand, designed as an analogue of **C** (see Figure 1) that could be prepared in three steps instead of eight. Ligands **4a**−**4e** are a subgroup in which only the alkyl ether length is varied. Ligands **4f**−**4h** are *n*-butyloxy (green) analogues of **4a**, **4c**, and **4e**. Ligands **4i** and **4j** were designed as more and less calamitic analogues of **4a**, respectively.

Our sequence of unoptimized reactions started with a benchtop Suzuki cross-coupling[26] between commercially available unprotected methoxybromophenols (**1**, R = CH_3) or 2-bromo-5-butoxyphenol (prepared by bromination of 3-butoxyphenol[27]) and three different commercially available areneboronic acids (blue), affording **2** in just 1 h.[28] The modest yields are due to competing proto-deborylation. Next, Boc-protected amino mesylates with alkyl spacers of 2, 3, 4, 6, or 12 carbons (red, purchased or prepared by mesylation of Boc-protected amino alcohols) are attached at the phenol oxygen on the phenol by nucleophilic substitution to afford **3**; yields are typically >70%. Finally, Boc deprotection affords the free amines **4a**−**4j** in near-quantitative yield without purification. All ligands were solids, although **4j** is low melting. Owing to the short reaction times and ease of purification of each step, ligands can be prepared within 48 h. Functional groups that proved more challenging for this sequence include (1) the ethylamine side arm found in **4d**, which is unstable prior to Boc protection; (2) the triaryl rod in **4i**, which is sparingly soluble in all steps; and (3) the ether-linked arene present in **4j**, which is more susceptible to proto-deborylation in the first step.

Of the ligands synthesized, **4a**−**4h** exhibit crystal morphologies as visualized by polarized optical microscopy (POM) and confirmed by differential scanning calorimetry (DSC) (Figure 2). Although **4c**, **4e**, and **4h** resemble smectic mesophase by POM, no evidence of a liquid crystal phase was detected: all ligands visually transition directly from crystal to isotropic liquid and do not shear when handling on glass. Crystallinity was confirmed by DSC, whereby only a single transition was observed for **4a**−**4h** (Figure 2, inset in each POM image) and which we ascribe to melting from the solid to the isotropic liquid phase (see the Supporting Information for DSC traces). In contrast, mesogens like **A**−**C** and others[29] exhibit multiple phase transitions by POM and DSC. Interestingly, ligand **4c** exhibited a higher melting point than any other ligand, which may be attributed to shorter alkyl chain lengths within the amine tether (red) and aryl ether (green). Similarly, ligand **4g** exhibits a higher melting point than **4f** and **4h**.

We attached ligands **4a**−**4c** and **4e**−**4h** to commercial 6.2 nm octadecylamine (ODA)-functionalized quantum dots (QDs) using the ligand exchange reaction previously reported by Murray and co-workers.[30] In the case of **4a**, ^{1}H NMR analysis of the QDs following ligand exchange revealed a 60:40 ratio of ligand **4a** to ODA bound on the QD's. Interestingly, in our previous study using ligand **C**, the same exchange procedure led to a 90:10 ratio.[10] Each of the ligand-modified quantum dots that we prepared readily dispersed in 4-cyano-4′-pentylbiphenyl above the clearing point (34 °C). Upon cooling from the isotropic to nematic phase, the ligand-modified QD's all spontaneously assemble into microcapsules similar to those previously observed using QD's modified with ligand **C**. The ligand is understood to promote uniform particle dispersion in the isotropic phase[8] and stabilize capsule formation via nematic phase templating.[9] Figure 3a shows a

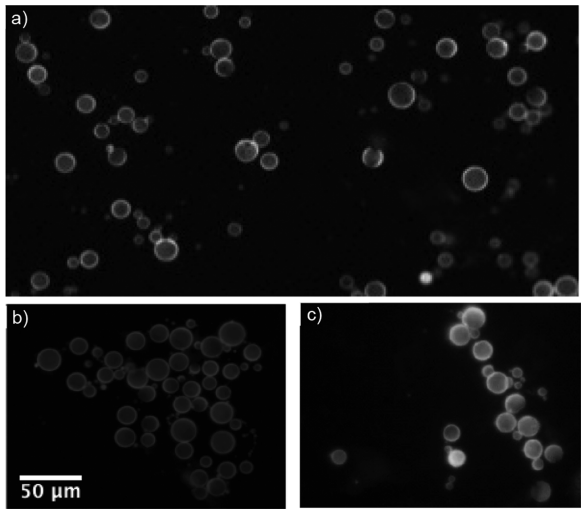

Figure 3. Same-slide ambient temperature fluorescence microscope images of QD mesostructures formed from 6.2 nm CdSe/ZnS QDs (λ_{max} = 540 nm) functionalized with ligand **4a** following dispersion in 4-cyano-4′-pentylbiphenyl (0.15 wt %) after (a) depositing on the slide, (b) reheating the slide through the clearing point, and (c) reheating the slide to 350 °C. Images record total fluorescence emission intensity following excitation at λ_{max} = 540 nm.

DOI: 10.1021/acsanm.9b00476
ACS Appl. Nano Mater. 2019, 2, 2542−2547

fluorescence microscope image of mesostructures formed using QD's functionalized with ligand **4a** (for other ligands, see the Supporting Information). Reheating to above the nematic phase clearing point of 34 °C and recooling did not destroy the capsules (Figure 3b), nor did heating to the maximum temperature allowed by our experimental setup (350 °C, Figure 3c). For comparison, QD's functionalized with ligand **C** decompose at just 120 °C.[9] The thermostability of QD's functionalized with **4a** bodes well for potential material applications.[21,31]

To further characterize the nanoscale morphology of the QD shells, scanning electron microscopy (SEM) images were captured. Figure 4 shows two representative SEM images from

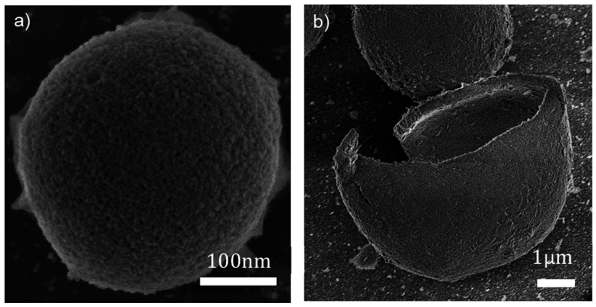

Figure 4. Scanning electron microscope images of (a) intact and (b) fractured QD capsules formed from 540 nm CdSe/ZnS QDs functionalized with ligand **4a**. These images were captured from a single sample grid.

the same sample grid: one of an intact shell composed of densely packed functionalized QD's (Figure 4a) and one of a fractured shell (Figure 4b). The latter confirms that the microstructure is indeed hollow, with a relatively thin wall. Approximately 15% of the shells observed using SEM are fractured, presumably as a result of mechanical shear during sample preparation. Mechanical methods can be used to break the capsules, using fast shearing for example. We propose that these novel ligands can be applied to high-temperature applications wherein encapsulation stability under high temperature is required. Such a property distinguishes these capsules from other, more temperature-sensitive encapsulation technologies such as polymersomes and liposomes or the thermally sensitive capsules from our group's earlier work.[11]

We next quantified nanoparticle packing in the shell wall using small-angle X-ray scattering (SAXS) measurements following our established method.[10] Figure 5 shows scattering intensity as a function of the scattering vector, q, which is related to average quantum dot separation within a shell wall, d, as $q = 2\pi/d$. For each sample, we observed a broad diffraction peak (the positions of which were determined by subtracting a baseline from the raw data and fitting a Gaussian). As shown in Figure 5, linker arm length has a significant effect on interparticle separation. The homologous series of ligands **4c**, **4b**, **4a**, and **4e**, employing 3-, 4-, 6-, and 12-carbon aminoalkyl linkers, respectively, afforded interdot separations of 10.15, 11.79, 12.94, and 13.25 nm—an apparent logarithmic correlation between interdot separation and aminoalkyl chain length (inset, Figure 5). Interestingly, when the ethereal arm (green, Table 1) is changed from CH_3 to C_4H_9, the aminoalkyl chain length no longer correlates to interparticle spacing; in fact, the ligand bearing the most

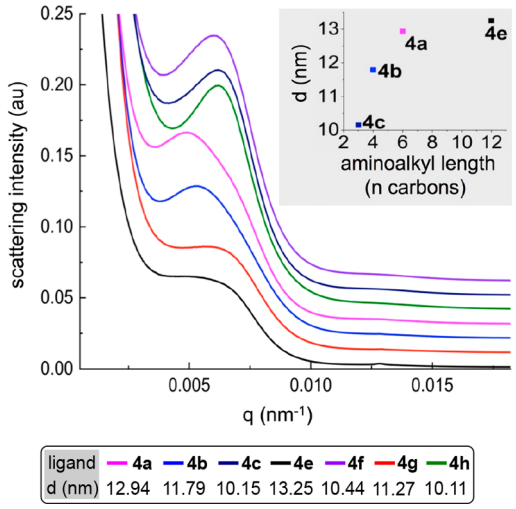

Figure 5. Small-angle X-ray scattering (SAXS) data collected at 10 keV with 1 s exposure for assembled quantum dot microshells suspended in nematic liquid crystal prepared at 0.15 wt % and plotted as relative intensity as a function of scattering vector, q. The characteristic interparticle spacing, d, is calculated from each peak position as $2\pi/q$.

aliphatic carbons that we evaluated (**4h**) affords microcapsules with the closest average interdot distance (10.11 nm).

In our previous work, quantum dot emission spectra and fluorescence lifetimes were characterized using drop-cast films and nanoparticle clusters in a liquid crystal.[32] Therein, we observed that mesogenic ligands of different alkyl chain lengths can be used to tune the quantum dot emission spectrum by modulating Forster resonance energy transfer (FRET) between quantum dots. In some cases, FRET could be avoided by using a ligand that produced an average nanoparticle spacing >10 nm. The SAXS data presented in Figure 5 underscore the potential utility of the new ligands. Additional possibilities for spectral modification may be possible, including by encapsulating dye molecules within the optically active capsules.[11]

Given the ability of the microcapsules to remain intact up to very high temperatures, for practical optical applications using quantum dots, thermal luminescence quenching becomes a concern. Isolated quantum dots lose luminescence intensity significantly at high temperatures, and irreversible quenching mechanisms can degrade performance over time under temperature cycling.[33] For example, in high-temperature applications such as high-power LEDs for lighting, the operating temperature can be up to 200 °C. To test for thermal quenching in the capsule geometry, we performed preliminary testing to characterize the effects of heating to 300 °C and cooling back to room temperature (Figure S-4). Although a degree of irreversible quenching is observed, the capsules retain some luminescence up to 300 °C. Loss of capping ligands at high temperatures is a well-known mechanism for irreversible quantum dot quenching, but in these capsules, wherein the ligands interact and stabilize, loss of capping ligands appears to be attenuated. A more detailed characterization of thermal quenching will be performed in future work to follow this paper as irreversible quenching can be a serious limitation in high-temperature QD applications.

DOI: 10.1021/acsanm.9b00476
ACS Appl. Nano Mater. 2019, 2, 2542−2547

CONCLUSIONS

In summary, we have developed a rapid, modular synthesis of new side-attaching calamitic promesogenic ligands. Their attachment to quantum dots and subsequent self-assembly in a liquid crystal host demonstrates the broad applicability of nematic templating. In addition to its modularity and scalability, the new ligand scaffold is noteworthy for its ability to deliver remarkably thermostable quantum dot microcapsules. Because of the unique thermal stability of our capsules, they may be well-suited for a wide range of applications in various fields, particularly encapsulations. Empowered by this scalable and modular ligand synthesis, future studies will endeavor to investigate the influence of ligand structure on shell formation, stability, and porosity.

EXPERIMENTAL SECTION

Preparation of the Amine Linkers (S1a−e). *General Procedure I.* Into a round-bottom flask charged with a PTFE-coated magnetic stir bar were added 1.0 equiv of alcohol in 0.2 M dry DCM and 1.3 equiv of triethylamine. The reaction mixture was placed in an ice bath, and 1.2 equiv of methanesulfonyl chloride was added dropwise. After 18 h, the reaction mixture was quenched with water and separated. The organic layer was dried over anhydrous sodium sulfate and removed under reduced pressure to afford **S1a−e**.

Preparation of the Rodlike Ligand Backbone via Suzuki Cross-Coupling (2a−d). *General Procedure II.* Into a 20 mL vial charged with a PTFE-coated magnetic stir bar were added 1.0 equiv of aryl bromide, 1.5 equiv of arylboronic acid, and 0.05 equiv of palladium(II) acetate. The vial was sealed with septa and placed under vacuum, and then it was filled with nitrogen. To this vial was added 0.5 M degassed water and 2.0 equiv of degassed diisopropylamine. The reaction mixture was stirred for an hour at 100 °C. The mixture was extracted with ethyl acetate and passed through a pad of Celite. The residue was then dried over anhydrous sodium sulfate and removed under reduced pressure. Purification by column chromatography (100:0 → 80:20 hexanes:EtOAc) on SiO_2 afforded **2a−d** as a solid.

Preparation of N-Boc-Protected Promesogenic Organic Ligands (3a−j). *General Procedure III.* Into a 20 mL vial charged with a PTFE-coated magnetic stir bar were added 1.0 equiv of **2**, 2.0 equiv of **S1**, and 2.0 equiv of potassium iodide in 0.075 M dry THF. 2.0 equiv of 1.7 M KO*t*-Bu in THF was added to the vial dropwise. The reaction mixture was capped and stirred for 12 h at 60 °C. The solvent was removed under reduced pressure, and the solid residue was extracted with water and DCM. The organic layer was collected and dried over anhydrous sodium sulfate and removed under reduced pressure. Purification by column chromatography (100:0 → 85:15 hexanes:ethyl acetae) on SiO_2 afforded **3a−j** as a solid.

Preparation of the Promesogenic Organic Ligands (4a−j). *General Procedure IV.* Into a 20 mL vial charged with a PTFE-coated magnetic stir bar were added 1.0 equiv of **3** in 0.1 M dry DCM. The reaction mixture was placed in an ice bath, and then 15 equiv of trifluoroacetic acid was added slowly. After 2 h, the reaction mixture was quenched with saturated sodium bicarbonate and extracted three times with DCM. The organic layer was passed through a pad of anhydrous sodium sulfate and removed under reduced pressure to afford **4a−j** as a solid.

Differential Scanning Calorimetry of Ligands. Small amounts (6−10 mg) of ligand in the crystal phase were encapsulated in an aluminum pan and cycled through melting and recrystallization at least once before recording a DSC trace. All data were collected on melting with a temperature ramp rate of 10 °C/min. An empty pan was used for the reference material. Enthalpies for each transition are calculated as the area under each peak.

Polarized Optical Microscopy Procedure. A thin film of each ligand was enclosed between a standard glass slide and coverslip and slowly heated to the isotropic phase. The films were then cooled into the crystal phase and reheated several times on a Linkham microscopy heating stage to identify a reversible phase sequence on the polarized optical microscope.

Ligand Exchange Process. For surface modification of quantum dots, we exchanged the ODA ligand with a mesogenic ligand (LC-QDs). This exchange involves 1 mL of quantum dot (CdSe/ZnS nanocrystal) solution with an octadecylamine ligand (ODA) attached and mixed with 1 mL of acetone. Free ligand was removed by centrifugation at 7000 rpm for 10 min. The supernatant was discarded, and then the last step was repeated again with the precipitate two times by adding 1 mL of acetone. Once washing is done, the precipitate was dissolved in 1 mL of chloroform and mixed with 1 mL solution of the synthesized ligand in chloroform (0.01 g/mL). ODA was then exchanged with the new ligand on the QD surface by heating at 40 °C and stirring the solution at 200 rpm for 5 h. The mixture was then removed from the heating stage and left to cool to room temperature. The free ligand was removed by washing it with 1 mL of ethyl acetate and centrifuged for 10 min and then washed again twice by adding 1 mL of ethyl acetate. For storage, the precipitate is taken up in 1 mL of toluene.

Microcapsule Formation Procedure. Microcapsules were prepared via nematic templating by heating 0.15 wt % of functionalized quantum dots in 4-cyano-4′-pentylbiphenyl above the nematic−isotropic transition point (34 °C) and then cooling back to the nematic phase in an Eppendorf tube. After gentle centrifugation, the shells were inserted into 1.5 mm borate glass X-ray capillaries and further centrifuged to form a pellet at the bottom of capillary.

Preparation for SEM Imaging. 0.2 μL of liquid-crystal-functionalized QDs mixture was pipetted onto a copper grid with 300 mesh carbon film, while holding the composite material at a temperature above the nematic−isotropic phase transition point. The grid was then cooled into the nematic phase, forming shells suspended in 5CB directly on the grid. Finally the 5CB was washed from the grid with acetone by pipetting a droplet onto the grid surface then wicking and evaporating the excess solvent.

ASSOCIATED CONTENT

Supporting Information

The Supporting Information is available free of charge on the ACS Publications website at DOI: 10.1021/acsanm.9b00476.

Experimental procedures and characterization data for ligand synthesis, ligand exchange onto commercial QD using **4a**, and all mesostructures (PDF)

AUTHOR INFORMATION

Corresponding Authors

*E-mail: lhirst@ucmerced.edu.

*E-mail: bstokes2@ucmerced.edu.

ORCID

Benjamin J. Stokes: 0000-0002-5982-654X

Notes

The authors declare the following competing financial interest(s): Patent application no. PCT/US2018/058271 has been filed.

ACKNOWLEDGMENTS

This research was supported by the National Science Foundation (CBET-1507551), by a grant from the University of California Cancer Research Coordinating Committee, by grants from the Merced Nanomaterials Center for Energy and Sensing (funded by NASA grant NNX15AQ01A), and by the UC Merced Committee on Research. We also thank the Beamline 7-3-3 staff at Lawrence Berkeley Lab for generous assistance with the Advanced Light Source, which is a DOE Office of Science User Facility (contract DE-AC02-05CH11231).

DOI: 10.1021/acsanm.9b00476
ACS Appl. Nano Mater. 2019, 2, 2542−2547

REFERENCES

(1) Hines, D. A.; Kamat, P. V. Recent Advances in Quantum Dot Surface Chemistry. *ACS Appl. Mater. Interfaces* **2014**, *6*, 3041−3057.
(2) Lewandowski, W.; Wójcik, M.; Górecka, E. Metal Nanoparticles with Liquid-Crystalline Ligands: Controlling Nanoparticle Superlattice Structure and Properties. *ChemPhysChem* **2014**, *15*, 1283−1295.
(3) Nealon, G. L.; Greget, R.; Dominguez, C.; Nagy, Z. T.; Guillon, D.; Gallani, J.-L.; Donnio, B. Liquid-Crystalline Nanoparticles: Hydrid Design and Mesophase Structures Beilstein. *Beilstein J. Org. Chem.* **2012**, *8*, 349−370.
(4) Yu, C. H.; Schubert, C. P. J.; Welch, C.; Tang, B. J.; Tamba, M.-G; Mehl, G. H. Design, Synthesis, and Characterization of Mesogenic Amine-Capped Nematic Gold Nanoparticles with Surface-Enhanced Plasmonic Resonances. *J. Am. Chem. Soc.* **2012**, *134*, 5076−5079.
(5) Mirzaei, J.; Reznikov, M.; Hegmann, T. Quantum dots as Liquid Crystal Dopants. *J. Mater. Chem.* **2012**, *22*, 22350−22365.
(6) Whitesides, G. M.; Grzybowski, B. Self-Assembly at all Scales. *Science* **2002**, *295*, 2418−2421.
(7) Prodanov, M. F.; Pogorelova, N. V.; Kryshtal, A. P.; Klymchenko, A. S.; Mely, Y.; Semynozhenko, V. P.; Krivoshey, A. I.; Reznikov, Y. A.; Yarmolenko, S. N.; Goodby, J. W.; Vashchenko, V. V. Thermodynamically Stable Dispersions of Quantum Dots in a Nematic Liquid Crystal. *Langmuir* **2013**, *29*, 9301−9309.
(8) Rodarte, A. L.; Nuno, Z. S.; Cao, B. H.; Pandolfi, R. J.; Quint, M. T.; Ghosh, S.; Hein, J. E.; Hirst, L. S. Tuning Quantum-Dot Organization in Liquid Crystals for Robust Photonic Applications. *ChemPhysChem* **2014**, *15*, 1413−1421.
(9) Rodarte, A. L.; Cao, B. H.; Panesar, H.; Pandolfi, R. J.; Quint, M.; Edwards, L.; Ghosh, S.; Hein, J. E.; Hirst, L. S. Self-Assembled Nanoparticle Micro-Shells Templated by Liquid Crystal Sorting. *Soft Matter* **2015**, *11*, 1701−1707.
(10) Riahinasab, S. T.; Elbaradei, A.; Keshavarz, A.; Stokes, B. J.; Hirst, L. S. Nanoparticle Microstructures Templated by Liquid Crystal Phase-Transition Dynamics. *Proc. SPIE* **2017**, *10125*, 1012503.
(11) Quint, M. T.; Sarang, S.; Quint, D. A.; Keshavarz, A.; Stokes, B. J.; Subramaniam, A. B.; Huang, K. C.; Gopinathan, A.; Hirst, L. S.; Ghosh, S. Plasmon-Actuated Nano-Assembled Microshells. *Sci. Rep.* **2017**, *7*, 17788.
(12) Melton, C.; Riahinasab, S.; Keshavarz, A.; Stokes, B.; Hirst, L. Phase Transition-Driven Nanoparticle Assembly in Liquid Crystal Droplets. *Nanomaterials* **2018**, *8*, 146.
(13) Costa-Fernández, J. M.; Pereiro, R.; Sanz-Medel, A. The Use of Luminescent Quantum Dots for Optical Sensing. *TrAC, Trends Anal. Chem.* **2006**, *25*, 207−218.
(14) Jaiswal, J. K.; Mattoussi, H.; Mauro, J. M.; Simon, S. M. Long-Term Multiple Color Imaging of Live Cells Using Quantum Dot Bioconjugates. *Nat. Biotechnol.* **2003**, *21*, 47−51.
(15) Dabbousi, B. O.; Rodriguez-Viejo, J.; Mikulec, F. V.; Heine, J. R.; Mattoussi, H.; Ober, R.; Jensen, K. F.; Bawendi, G. (CdSe)ZnS Core-Shell Quantum Dots: Synthesis and Characterization of a Size Series of Highly Luminescent Nanocrystallites. *J. Phys. Chem. B* **1997**, *101*, 9463−9475.
(16) Brus, L. Quantum Crystalline and Nonlinear Optics. *Appl. Phys. A: Solids Surf.* **1991**, *53*, 465−474.
(17) Nozik, A. J. Quantum Dot Solar Cells. *Phys. E* **2002**, *14*, 115−120.
(18) Dayal, S.; Kopidakis, N.; Olson, D. C.; Ginley, D. S.; Rumbles, G. *Nano Lett.* **2010**, *10*, 239−242.
(19) Munro, A. M.; Bardecker, J. A.; Liu, M. S.; Cheng, Y.-J.; Niu, Y.-H.; Plante, I. J-L.; Jen, A. K.-Y.; Ginger, D. S. Colloidal CdSe Quantum Dot Electroluminescence: Ligands and Light-emitting diodes. *Microchim. Acta* **2008**, *160*, 345−350.
(20) Lewandowski, W.; Jatczak, K.; Pociecha, D.; Mieczkowski, J. Control of Gold Nanoparticle Superlattice Properties via Mesogenic Ligand Architecture. *Langmuir* **2013**, *29*, 3404−3410.
(21) Mang, X.; Zeng, X.; Tang, B.; Liu, F.; Ungar, G.; Zhang, R.; Cseh, L.; Mehl, G. H. Control of Anisotropic Self-Assembly of Gold Nanoparticles Coated with Mesogens. *J. Mater. Chem.* **2012**, *22*, 11101−11106.
(22) Zeng, X.; Liu, F.; Fowler, A. G.; Ungar, G.; Cseh, L.; Mehl, G. H.; Macdonald, J. E. 3D Ordered Gold Strings by Coating Nanoparticles with Mesogens. *Adv. Mater.* **2009**, *21*, 1746−1750.
(23) Hegmann and co-workers used a silane analogue as a proligand to thiol B: Umadevi, S.; Feng, X.; Hegmann, T. Large Area Self-Assembly of Nematic Liquid-Crystal-Functionalized Gold Nanorods. *Adv. Funct. Mater.* **2013**, *23*, 1393−1403.
(24) Hegmann's proligand is closely related to the dimeric siloxane-bridged compound reported by Dunmur and co-workers Diez, S.; Dunmur, D. A.; Rosario De La Fuente, M.; Karahaliou, P. K.; Mehl, G.; Meyer, T.; Ángel, P. z. J. M.; Photinos, D. J. Dielectric Studies of a Laterally-Linked Siloxane Ester Dimer. *Liq. Cryst.* **2003**, *30*, 1021−1030.
(25) Riahinasab, S. T.; Keshavarz, A.; Melton, C. N.; Elbaradei, A.; Warren, G. I.; Selinger, R. L. B.; Stokes, B. J.; Hirst, L. S. Nanoparticle-Based Hollow Microstructures Formed by Two-Stage Nematic Nucleation and Phase Separation. *Nat. Commun.* **2019**, *10*, 894.
(26) Liu, C.; Zhang, Y.; Liu, N.; Qiu, J. A Simple and Efficient Approach for the Palladium-Catalyzed Ligand-Free Suzuki Reaction in Water. *Green Chem.* **2012**, *14*, 2999−3003.
(27) Hemelaere, R.; Carreaux, F.; Carboni, B. A Diastereoselective Route to *Trans*-2-Aryl-2,3-dihydrobenzofurans through Sequential Cross-Metathesis/Isomerization/Allylboration Reactions: Synthesis of Bioactive Neolignans. *Eur. J. Org. Chem.* **2015**, *2015*, 2470−2481.
(28) For an alternative high-yielding Suzuki cross-coupling method between substrates bearing long-chain oxyalkyl groups, see: Vashchenko, V.; Krivoshey, A.; Knyazeva, I.; Petrenko, A.; Goodby, J. W. Palladium-Catalyzed Suzuki Cross-Coupling Reactions in a Microemulsion. *Tetrahedron Lett.* **2008**, *49*, 1445.
(29) Getmanenko, Y. A.; Twieg, R. J. Unprecedented Negishi Coupling at C-Br in the Presence of a Stannyl Group as a Convenient Approach to Pyridinylstannanes and their Application in Liquid Crystal Synthesis. *J. Org. Chem.* **2008**, *73*, 830−839.
(30) Hostetler, M. J.; Green, S. J.; Stokes, J. J.; Murray, R. W. Monolayers in Three Dimensions: Synthesis and Electrochemistry of ω-Functionalized Alkanethiolate-Stabilized Gold Cluster Compounds. *J. Am. Chem. Soc.* **1996**, *118*, 4212−4213.
(31) Nguyen, T. D.; Jankowski, E.; Glotzer, S. C. Self-Assembly and Reconfigurability of Shape-Shifting Particles. *ACS Nano* **2011**, *5*, 8892−8903.
(32) Amaral, J. J.; Betady, E.; Quint, M. T.; Martin, D.; Riahinasab, S. T.; Hirst, L. S.; Ghosh, S. Effect of Mesogenic Ligands on Short and Long-Term Spectral Dynamics and Stability of Core-Shell CdSe/ZnS Quantum Dots. *Mater. Res. Express* **2016**, *3*, 105029.
(33) Zhao, Y.; Riemersma, C.; Pietra, F.; Koole, R.; De Mello Donegá, C.; Meijerink, A. High-Temperature Luminescence Quenching of Colloidal Quantum Dots. *ACS Nano* **2012**, *6*, 9058−9067.

DOI: 10.1021/acsanm.9b00476
ACS Appl. Nano Mater. 2019, 2, 2542−2547